Review of Scientific Instruments

Initial operation of perpendicular line-of-sight compact neutron emission spectrometer in the large helical device

Cite as: Rev. Sci. Instrum. **93**, 093504 (2022); https://doi.org/10.1063/5.0100494
Submitted: 24 May 2022 • Accepted: 10 August 2022 • Published Online: 12 September 2022

S. Sangaroon, K. Ogawa and M. Isobe

Review of Scientific Instruments ARTICLE scitation.org/journal/rsi

Initial operation of perpendicular line-of-sight compact neutron emission spectrometer in the large helical device

Cite as: Rev. Sci. Instrum. 93, 093504 (2022); doi: 10.1063/5.0100494
Submitted: 24 May 2022 • Accepted: 10 August 2022 •
Published Online: 12 September 2022

S. Sangaroon,[1,a)] K. Ogawa,[2,3] and M. Isobe[2,3]

AFFILIATIONS

[1] Energy Research Unit, Department of Physics, Faculty of Science, Mahasarakham University, Maha Sarakham 44150, Thailand
[2] National Institute for Fusion Science, National Institutes of Natural Sciences, Toki 509-5292, Japan
[3] The Graduate University for Advanced Studies, SOKENDAI, Toki 509-5292, Japan

[a)] **Author to whom correspondence should be addressed:** siriyaporn.s@msu.ac.th

ABSTRACT

The perpendicular line-of-sight compact neutron emission spectrometer (perpendicular CNES) was newly installed to understand the helically trapped fast-ion behavior through deuterium–deuterium (D–D) neutron energy spectrum measurement in the Large Helical Device (LHD). The energy calibration of the EJ-301 liquid scintillation detector system for perpendicular CNES was performed on an accelerator-based D–D neutron source. We installed two EJ-301 liquid scintillation detectors, which view the LHD plasma vertically from the lower side through the multichannel collimator. The D–D neutron energy spectrum was measured in a deuterium perpendicular-neutral-beam-heated deuterium plasma. By the derivative unfolding technique, it was found that the D–D neutron energy spectrum had a double-humped shape with peaks at ~2.33 and ~2.65 MeV. D–D neutron energy spectrum was calculated based on the fast ion distribution function using guiding center orbit-following models considering the detector's energy resolution. The calculated peak energies in the D–D neutron energy spectrum almost match the experiment. In addition, a feasibility study toward the measurement of the energy distribution of ion-cyclotron-range-of-frequency-wave-accelerated beam ions was performed.

I. INTRODUCTION

In present-day fusion plasma experiments, plasmas are mainly heated by fast ions generated by neutral beam injection (NBI) and/or ion cyclotron range of frequency (ICRF) waves. Understanding the fast-ion's behavior is therefore crucial for achieving higher-performance plasmas.[1] At the same time, the pressure of fast ions can be a free energy source to excite fast-ion-driven magnetohydrodynamic (MHD) instabilities, which might cause the enhanced transport of fast ions.

The comprehensive set of neutron diagnostics providing fast-ion information has been working in the Large Helical Device (LHD) since March 2017.[2–5] Confinement of passing and helically trapped beam ions in MHD quescient plasmas has been studied by the decay time of total neutron emission rate S_n in short pulse deuterium NBI experiments using the neutron flux monitor (NFM).[6] It was reported that the confinement of beam ions becomes better with an inward shift of the magnetic axis.[7] For the fast-ion-driven MHD instability study, radial transport of helically trapped beam ions due to fast-ion-driven MHD instability has been visualized[8,9] using vertical neutron cameras.[10,11] For a deeper understanding of the classical confinement of fast ions and the excitation mechanism of the fast-ion-driven MHD instabilities, information on the fast ion energy distribution is additionally required.

To understand the energy distribution of fast ions, we have been developing neutron energy spectrometers in LHD.[12] Since 2020, the tangential line-of-sight compact neutron emission spectrometer (tangential CNES) has been operating.[13] Significant Doppler shift in deuterium–deuterium (D–D) neutron energy reflecting the energy distribution of passing beam ions injected by negative-ion-source-based tangential NBI (N-NB) has been reported.[14,15] In 2021, to understand helically trapped beam ion

energy distribution, a new perpendicular line-of-sight CNES (perpendicular CNES) was installed. In this paper, we report the details and initial operation of perpendicular CNES. The conventional liquid organic scintillator is used for the perpendicular CNES due to its relatively fast decay time (~ns), thus, the perpendicular CNES can operate during the high S_n. Liquid organic scintillation detectors have become important in fusion devices for fast neutron spectroscopy due to their relatively high light output, good detection efficiency, fast decay time, and excellent n/γ pulse shape discrimination capabilities.[16,17] Together with a suitable unfolding technique, the CNES based on a liquid scintillator can provide a high-resolution neutron spectrometer.

II. THE CHARACTERIZATION OF EJ-301 LIQUID SCINTILLATION DETECTER SYSTEM

The energy calibration of the EJ-301 liquid scintillation detecter system used for perpendicular CNES was performed using an accelerator-based neutron source in the fast neutron laboratory (FNL) of Tohoku University[18] [Fig. 1(a)]. The system is composed of an EJ-301 liquid scintillation detector and fast digital data acquisition (DAQ). The EJ-301 scintillator,[19] 1 in. in diameter and in height, is directly coupled to a 1 in. photomultiplier tube (PMT) (H10580-100-01, Hamamatsu Photonics K.K.).[20] The anode signal of the detector is fed into the fast DAQ (APV8102-14MWPSAGb, Techno AP Corp.).[21] The deuteron beam with 1.5, 2.0, and 3.0 MeV was respectively injected into the D_2 gas target to obtain a rather monoenergetic D–D neutron. The EJ-301 scintillation detector was placed at 15.5°, 60.8°, and 85.9° from the beam axis [Fig. 1(b)], where the D–D neutron energy peak at the detector position was expected to be ~2.5 to ~5.5 MeV. Pulse shape discrimination PSD = $(Q_{total} - Q_{fast})/Q_{total}$, where Q_{total} is an integrated signal in t_{total} of 34 ns and Q_{fast} is an integrated signal in t_{fast} of 10 ns, is used for discriminating fast-neutron and γ-ray [Figs. 1(c) and 1(d)]. In this neutron energy range, neutron-proton elastic scattering mainly occurs with the EJ-301 scintillator. The relation between the recoiled proton energy E_p and Q_{total}: E_p (MeV) = 0.22 × Q_{total} + 0.98 was obtained using maximum Q_{total} and expected D–D neutron energy peak at the detector position.

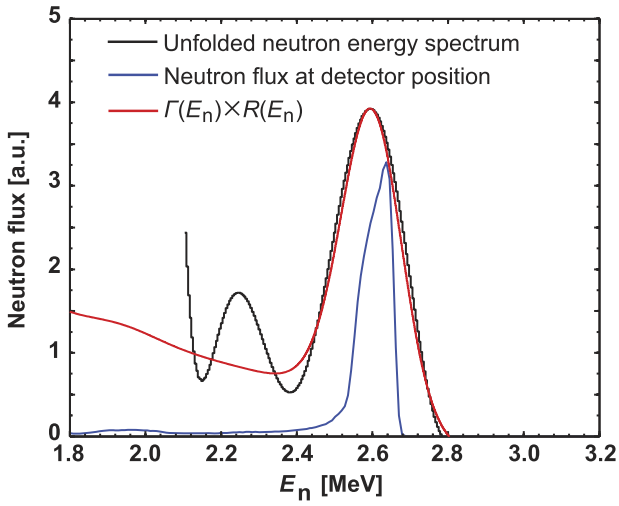

FIG. 2. Comparison of unfolded neutron energy spectrum, neutron flux at detector position, and calculated neutron energy spectrum when the detector's energy resolution is taken into account when a deuteron beam with an energy of 1.5 MeV was injected into the D_2 gas target and the detector was placed at 85.9° from the beam axis.

The unfolding of the D–D neutron energy spectrum $\phi(E_n)$ from E_p distribution was performed using the experimental results in the 1.5 MeV deuteron beam and 85.9° detector position case. The derivative unfolding[22] using $\phi(E_n) = \frac{-E_p}{TnV\sigma(E_p)}\left[y'(x)\{gL'(E_p)\}^2 + y(x)gL''(E_p)\right]$ was conducted. Here, T, n, V, σ, $y(x)$, g, $L(E_p)$, $'$, and $''$ represent the time duration, the density of hydrogen atom, the detector volume, the neutron-proton elastic scattering cross section, Q_{total} histogram, the PMT gain 6.6×10^5, light output as a function of the recoil particle energy,[23] the

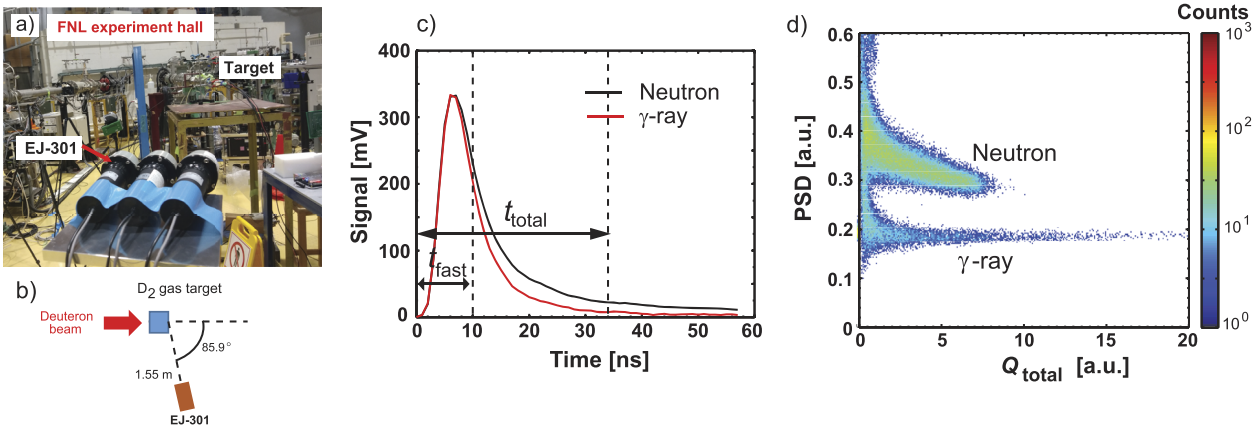

FIG. 1. (a) Arrangement of FNL experiment. (b) Schematic top view of the FNL D–D experiment where the detector is placed at 85.9° from the beam axis. (c) The typical neutron and γ-ray induced signal measured by the EJ-301 scintillation detector. (d) Two-dimensional PSD plot.

first derivative, and the second derivative, respectively. Note that the detection efficiency is not considered in this calculation. The black line in Fig. 2 shows the unfolded $\phi(E_n)$. Due to the derivative unfolding technique based on the data of the density of hydrogen atom, the detector volume, the neutron-proton elastic scattering cross-section, the PMT gain, and light output as a function of the recoil particle energy, the error bar of unfolded $\phi(E_n)$ is neglectable in this work. The energy resolution of the EJ-301 liquid scintillation detecter system $R(E_n)$ was evaluated by comparing experimentally obtained $\phi(E_n)$ and the calculated neutron flux $\Gamma(E_n)$ at the detector position. Here, the deuteron beam's energy spectrum in the D_2 gas target and the neutron transport in the FNL experiment hall was estimated by TRIM code[24] and Monte Carlo N-Particle transport (MCNP) code,[25] respectively. Here, $R(E_n) = \sqrt{a^2 + b^2/E_n + c^2/E_n^2}$ was assumed according to Ref. 26. Coefficients $a = 0.046$, $b = 0.069$, and $c = 0.009$ were determined through iterations that $\Gamma(E_n) \times R(E_n)$ matched experimentally obtained $\phi(E_n)$ (Fig. 2). It is worth noting that $R(E_n)$ was gradually changed from 7% to 6% in E_n from 1.8 to 3.2 MeV. The discrepancy in neutron energy spectrum at E_n below ~2.4 MeV might be caused by the scattered neutron effect.

III. MEASUREMENT OF D-D NEUTRON ENERGY SPECTRUM IN P-NB HEATED DEUTERIUM PLASMA IN LHD

We installed the EJ-301 liquid scintillation detector system in LHD. Two EJ-301 scintillation detectors are placed below the multichannel collimator and view the plasma vertically from the lower

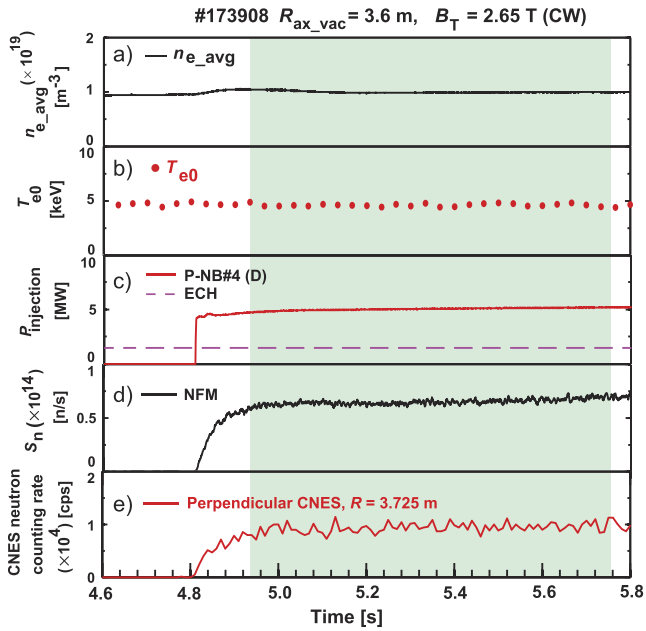

FIG. 4. Time evolution of deuterium plasma discharge No. 173908 performed in LHD. (a) Line-averaged electron density n_{e_avg}. (b) Central electron temperature T_{e0}. (c) P-NB#4 is injected during the selected time. (d) S_n measured by NFM. (e) Neutron counting rate measured with a perpendicular CNES at R of 3.275 m. The time interval between 4.93 and 5.75 s is selected (green-shaded).

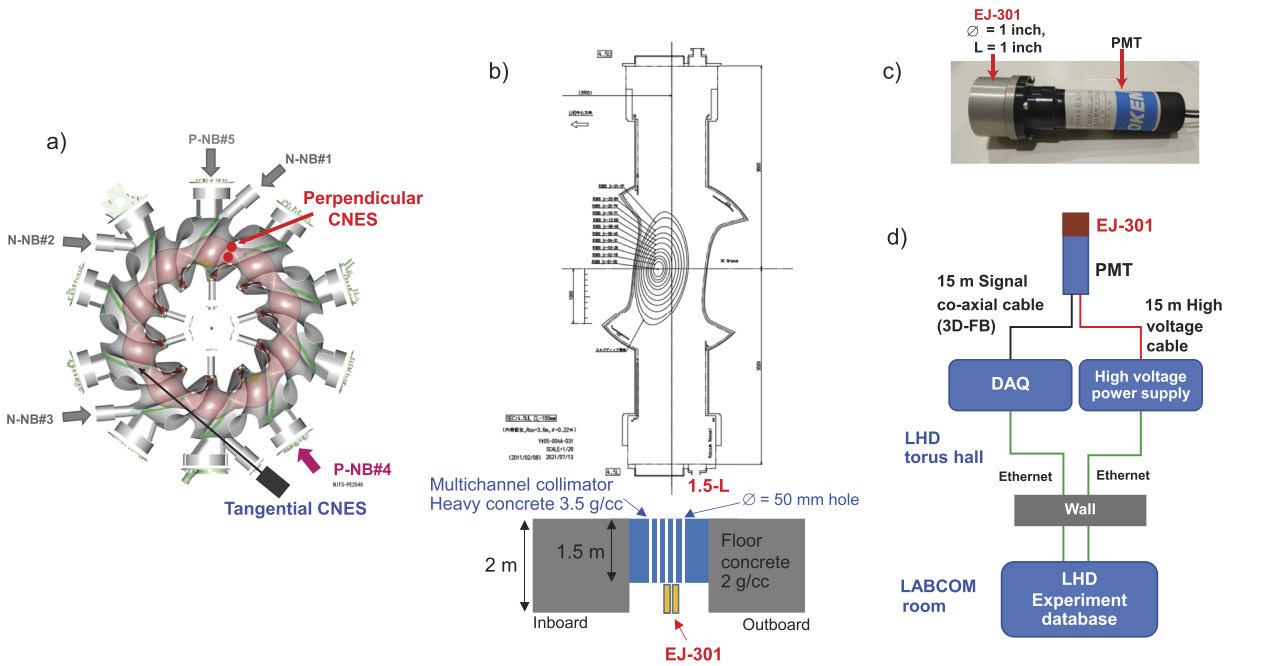

FIG. 3. (a) A schematic top view of LHD, P-NB#4, and CNESs. (b) A schematic drawing of the LHD cut view at the 1.5-L port and the perpendicular CNES. (c) EJ-301 liquid scintillation detector. (d) Electronics schematic of perpendicular CNES.

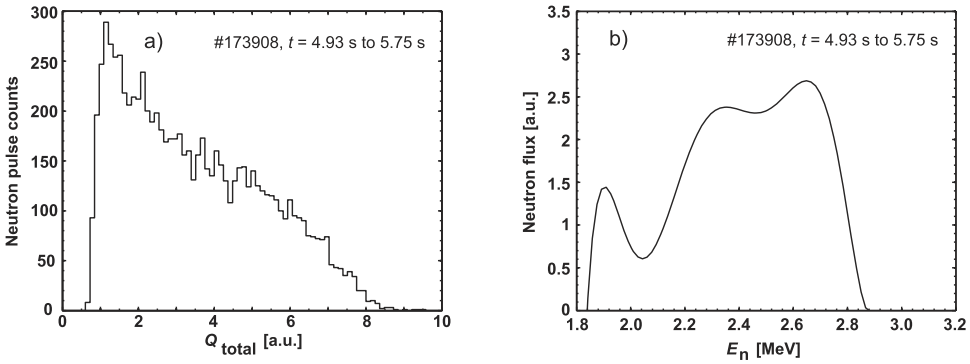

FIG. 5. (a) Histogram of the Q_{total} and (b) unfolded D–D neutron energy spectrum measured by perpendicular CNES, when the detector is at R = 3.725 m, performed in P-NB heated deuterium plasma discharge No. 173908.

side at the 1.5-L port (Fig. 3). The radial positions (R) of the detectors are 3.725 and 3.875 m, respectively. The detectors are biased with a high voltage (APV3304, Techno AP Corp.).[27] The digitized data obtained by DAQ is transferred to the LHD experiment database via 1 Gbps ethernet.

Measurement of D–D neutron energy spectrum by perpendicular CNES was conducted in P-NB heated deuterium plasma discharge No. 173908 (Fig. 4). In the experiment, the magnetic axis position in vacuum R_{ax_vac} was 3.60 m, and the toroidal magnetic field strength B_T was set to be 2.65 T with clockwise (CW) directions viewed from the top. P-NB#4 was injected continuously with energy of ~50 keV and power of ~5 MW. The neutron counting rate measured by the perpendicular CNES (R = 3.725 m) shows the same trend as S_n. Here, neutron pulses are discriminated using the PSD method. A time interval from 4.93 to 5.75 s was selected for D–D neutron energy spectrum analysis, where the bulk plasma parameters were almost unchanged. We unfolded $\phi(E_n)$ from the Q_{total} histogram measured by the perpendicular CNES [Fig. 5(a)] using the derivative unfolding method. It was shown that the unfolded $\phi(E_n)$ has a double-humped shape, with peaks at ~2.33 and ~2.65 MeV [Fig. 5(b)]. Two peaks might correspond to the Larmor motion of perpendicular beam ion.[28]

IV. COMPARISON OF D–D NEUTRON ENERGY SPECTRUM IN EXPERIMENT AND CALCULATION

The numerical simulation based on the orbit following model was performed to understand the D–D neutron energy spectrum measured in the P-NB heated plasma. The three-dimensional MHD equilibrium was reconstructed by VMEC2000 code[29] using the pressure profile given by real-time magnetic coordinate mapping system (TSMAP).[30] The beam deposition calculation HFREYA code[31,32] was utilized to calculate the birth position of the beam ions generated by P-NB. The guiding-center orbits of the 10^5 P-NB ions in the Boozer coordinates were followed within 1 s by the DELTA5D code.[33] D–D neutron energy spectrum expected to be obtained by perpendicular CNES is calculated by considering the beam ion energy distribution, Larmor phase, and detector's energy resolution (Fig. 6).

Beam ion energy distribution of deuterium plasma discharge No. 173908 at time t = 5.3 s integrated over perpendicular CNES sightline obtained by DELTA5D code is shown in Fig. 7(a). Figure 7(b) shows the calculated D–D neutron energy spectrum obtained by perpendicular CNES. The calculated $\phi(E_n)$ has a double humped shape with the peaks at ~2.33 and ~2.65 MeV. Although the relative height of the two peaks shows different characteristics, the peak energies agree with the experiment. The discrepancy in the relative height of two peaks and the understanding of a peak at 1.9 MeV obtained in the experiment are our future work. Furthermore, the effects of two sightlines of perpendicular CNES on the D–D neutron energy spectra will be discussed in future work.

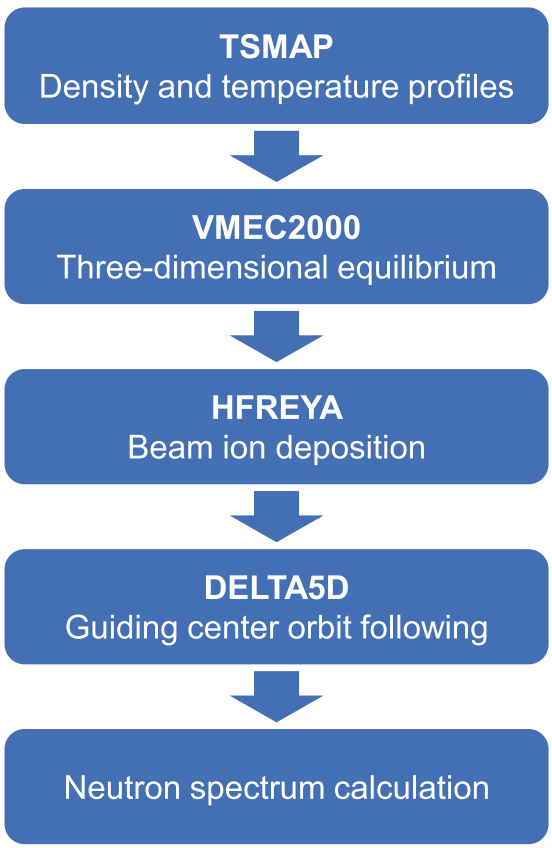

FIG. 6. Flowchart of the setup for D–D neutron energy spectrum calculations.

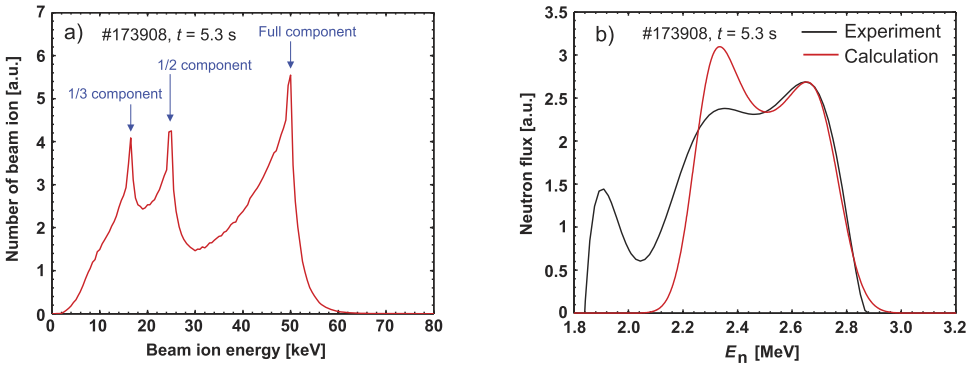

FIG. 7. (a) Beam ion energy distribution integrated over the perpendicular CNES sightline and (b) D–D neutron energy spectrum obtained by perpendicular CNES, when the detector is at R = 3.725 m, in the experiment and calculation.

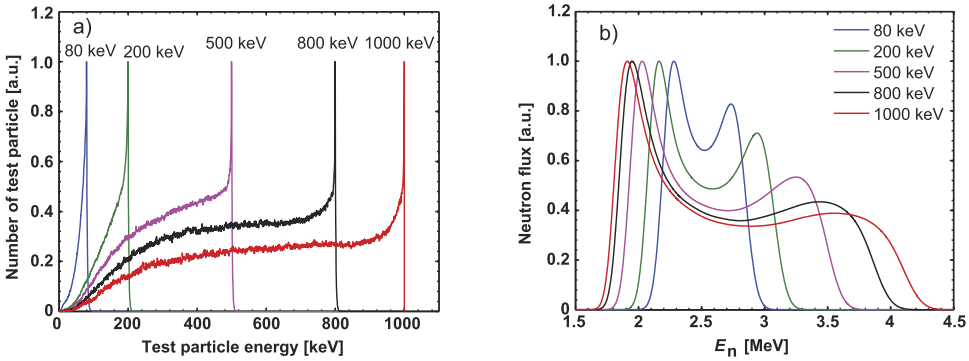

FIG. 8. (a) Test particle energy distribution integrated over the perpendicular CNES sightline and (b) D–D neutron energy spectrum expected to be obtained by perpendicular CNES when the detector is at R = 3.725 m.

V. FEASIBILITY STUDY TOWARD D–D NEUTRON ENERGY SPECTRUM MEASUREMENT IN ICRF WAVE AND NBI HEATED PLASMA

A feasibility study toward D–D neutron energy spectrum measurement in ICRF-wave- and NBI-heated deuterium plasmas was performed. In such experiments, beam ions can be accelerated by the ICRF wave. The measurement of the energy distribution of the ions through the D–D neutron energy spectrum could contribute to understanding the acceleration process. In this study, we used a simple model where the test particles were assumed to have the beam ion slowing down distribution, and we changed the initial test particle energy from 80 to 1000 keV. Test particle energy distributions integrated over perpendicular CNES sightline calculated by DELTA5D code for each case are shown in Fig. 8(a). Figure 8(b) shows the D–D neutron energy spectrum obtained by perpendicular CNES. The neutron energy spectrum expected to be obtained by perpendicular CNES shows that the peak locations shifted according to the test particle energy. The perpendicular CNES can be a candidate diagnostic for studying beam ion acceleration by ICRF wave.

VI. SUMMARY

Perpendicular line-of-sight CNES was newly installed to understand the behavior of helically trapped fast ions in the LHD. The energy calibration of the EJ-301 liquid scintillation detector system used for the perpendicular CNES was performed at an accelerator-based neutron source. We measured the D–D neutron energy spectrum by the perpendicular CNES in a deuterium P-NB heated LHD plasma. It was shown that the D–D neutron energy spectrum has a double-humped shape with peaks at ~2.33 and ~2.65 MeV using the derivative unfolding method. A neutron energy spectrum calculation based on the orbit following model was performed. The peak positions of the calculated neutron energy spectrum agree with the experiment. A feasibility study toward an understanding of beam ion acceleration by ICRF wave was performed. The perpendicular CNES might contribute to understanding the beam ion acceleration process.

ACKNOWLEDGMENTS

This research was supported by NIFS Collaboration Research Programs (Grant No. KOAH037), the NINS program of Promoting Research, Networking among Institutions (Grant No. 01411702), NSRF via the Program Management Unit for Human Resources and Institutional Development, Research and Innovation (Grant No. B05F640224), and Thailand Science Research and Innovation (TSRI) via Fundamental Fund FY2565 (Contract No. 2589646). We are pleased to acknowledge the assistance of the LHD Experiment Group.

AUTHOR DECLARATIONS

Conflict of Interest

The authors have no conflicts to disclose.

Author Contributions

S. Sangaroon: Conceptualization (equal); Formal analysis (equal); Investigation (equal); Methodology (equal); Validation (equal). **K. Ogawa**: Conceptualization (equal); Investigation (equal); Methodology (equal); Supervision (equal); Validation (equal). **M. Isobe**: Conceptualization (equal); Investigation (equal); Methodology (equal); Supervision (equal); Validation (equal).

DATA AVAILABILITY

The LHD data that support the findings of this study are openly available in LHD data repository at https://www-lhd.nifs.ac.jp/pub/Repository_en.html.

REFERENCES

[1] A. Fasoli *et al.*, Nucl. Fusion **47**, S264 (2007).
[2] M. Isobe *et al.*, IEEE Trans. Plasma Sci. **46**, 2050 (2018).
[3] M. Isobe *et al.*, Nucl. Fusion **58**, 082004 (2018).
[4] K. Ogawa *et al.*, Nucl. Fusion **59**, 076017 (2019).
[5] K. Ogawa *et al.*, Plasma Fusion Res. **16**, 1102023 (2021).
[6] M. Isobe *et al.*, Rev. Sci. Instrum. **85**, 11E114 (2014).
[7] H. Nuga *et al.*, J. Plasma Phys. **86**, 815860306 (2020).
[8] K. Ogawa *et al.*, Nucl. Fusion **58**, 044001 (2018).
[9] K. Ogawa *et al.*, Nucl. Fusion **60**, 112011 (2020).
[10] K. Ogawa *et al.*, Rev. Sci. Instrum. **89**, 113509 (2018).
[11] S. Sangaroon *et al.*, Rev. Sci. Instrum. **91**, 083505 (2020).
[12] M. Isobe *et al.*, Plasma Fusion Res. **17**, 2402008 (2022).
[13] M. Isobe *et al.*, J. Instrum. **17**, C03036 (2022).
[14] S. Sangaroon *et al.*, J. Instrum. **16**, C12025 (2021).
[15] S. Sangaroon *et al.*, AAPPS Bull. **32**, 5 (2022).
[16] A. Zimbal *et al.*, Rev. Sci. Instrum. **75**, 3553 (2004).
[17] F. Belli *et al.*, IEEE Trans. Nucl. Sci. **59**, 2512 (2012).
[18] M. Baba *et al.*, Nucl. Instrum. Methods Phys. Res., Sect. A **376**, 115–123 (1996).
[19] See https://eljentechnology.com/products/liquid-scintillators/ej-301-ej-309 for the specification of the EJ-301 scintillator.
[20] See https://www.hamamatsu.com/resources/pdf/etd/High_energy_PMT_TPMZ0003E.pdf for H10580-100-01 for the photomultiplier tube.
[21] See http://www.techno-ap.com/img/APV8102-14MWPSAGb_e.pdf for DAQ system.
[22] D. Slaughter and R. Strout, Nucl. Instrum. Methods Phys. Res. **198**, 349–355 (1982).
[23] V. V. Verbinski *et al.*, Nucl. Instrum. Methods **65**, 8–25 (1968).
[24] See http://www.srim.org/ for TRIM code.
[25] D. B. Pelowits, Report No. LA-CP-13-00634, Los Alamos National Laboratory, 2013.
[26] G. Dietze and H. Klein, Nucl. Instrum. Methods **193**, 549–556 (1982).
[27] See http://www.techno-ap.com/img/APV3304_e.pdf for the APV3304 high voltage power supply board.
[28] J. Eriksson *et al.*, Plasma Phys. Controlled Fusion **55**, 015008 (2013).
[29] S. P. Hirshman and O. Betancourt, J. Comput. Phys. **96**, 99 (1991).
[30] C. Suzuki *et al.*, Plasma Phys. Controlled Fusion **55**, 014016 (2013).
[31] S. Murakami *et al.*, Fusion Technol. **27**, 256 (1995).
[32] P. Vincenzi *et al.*, Plasma Phys. Controlled Fusion **58**, 125008 (2016).
[33] D. A. Spong *et al.*, Phys. Plasmas **18**, 056109 (2011).